Korean J. Chem. Eng., 35(2), 574-578 (2018)
DOI: 10.1007/s11814-017-0279-7

pISSN: 0256-1115
eISSN: 1975-7220

Deep-ultraviolet photodetector based on exfoliated n-type β-Ga_2O_3 nanobelt/p-Si substrate heterojunction

Gahyun Shin*,, Hong-Yeol Kim**, and Jihyun Kim*,**,†**

*Department of Nano-photonics Engineering, Korea University, Seoul 02841, Korea
**Department of Chemical and Biological Engineering, Korea University, Seoul 02841, Korea
(*Received 2 August 2017 • accepted 2 October 2017*)

Abstract−Low-dimensional semiconductor p-n junctions as components for optoelectronic devices are considered to be more promising than thin film equivalents. We fabricated heterojunction p-n solar blind photodiodes with the configuration of n-type β-Ga_2O_3 nanobelts contacted onto p-Si substrates. The junction between β-Ga_2O_3 and Si was formed by van der Waals interactions. The fabricated heterojunction p-n diodes exhibited typical rectifying current–voltage characteristics, with a rectification ratio as high as 1.56×10^4 at ±20 V and an ideality factor of approximately eight. Photoresponsive measurements showed that the heterojunction p-n diodes had a high sensitivity and selectivity for light at a wavelength of 254 nm, with fast response and decay characteristics. For the fast-response components, the response time constant was 4.06 s and the decay time constant was 0.16 s. The exfoliated β-Ga_2O_3 nanobelt/Si p-n heterojunction presented here constitutes a functional unit for low-dimensional ultra-wide bandgap electronic and optoelectronic devices.

Keywords: β-Ga_2O_3, Nanobelt, Solar-blind Photodiode, p-n Heterojunction, van der Waals Interaction

INTRODUCTION

β-Ga_2O_3 has attracted considerable attention as a next-generation high-power semiconductor material because of its ultra-wide energy bandgap of ~4.9 eV (direct) [1,2]. It is chemically and physically stable and its optical transparency at visible to deep ultraviolet (UV) wavelengths makes it particularly applicable to solar blind photodetectors. Moreover, β-Ga_2O_3 can be grown with a single crystalline bulk substrate (monoclinic) [3]. Bulk β-Ga_2O_3 substrates fabricated by edge-defined film-fed growth (EFG) are commercially available in sizes up to 2" and plates with dimensions of 4" and 6" are in development. There has also been progress in epitaxial growth techniques, including metalorganic chemical vapor deposition, hydride vapor phase epitaxy, and molecular beam epitaxy with controlled n-type doping over the range 10^{15}-10^{19} cm^{-3} using shallow donors (Sn or Si) [4]. With its numerous advantages, β-Ga_2O_3 is suitable for high-voltage power devices and UV optoelectronics. Higashiwaki et al. demonstrated β-Ga_2O_3-based power devices by fabricating metal-semiconductor field-effect transistors and metal oxide-semiconductor field-effect transistors [3,5,6]. UV photodetectors and light-emitting diodes based on β-Ga_2O_3 with different structures have also been investigated [7-10].

Low-dimensional semiconductors have more attractive features than thin film semiconductors, such as improved crystallinity and quantum confinement effects [11-13]. Dislocation-free single crystal GaN nanowire LEDs were reported whereby the emission wavelength could be tuned from 365 to 600 nm. β-Ga_2O_3 nanostructures such as nanowires [14], nanobelts [15-17], and nanosheets [18] have been synthesized. Interestingly, β-Ga_2O_3 nanostructures can also be obtained by mechanical exfoliation even though β-Ga_2O_3 only contains covalent bonds in its structure. There has not been a clear explanation yet, but it is commonly accepted that large differences in lattice constants allows β-Ga_2O_3 to be exfoliated to form nanostructures. An important advantage of mechanical exfoliation and transfer of low dimensional materials is the ease with which heterostructures can be formed with arbitrary substrates. Mechanical exfoliation also enables two or more materials to be stacked together through van der Waals interactions without lattice-induced strain. For example, Lee et al. demonstrated field-effect transistors by mechanically stacking graphene, hexagonal boron nitride (hBN), and molybdenum disulfide (MoS_2) [19]. The van der Waals heterostructure commonly has an abrupt transition between the stacked materials and a sharp gradient of carrier concentrations across the interface [20].

In this study, we demonstrate a p-n heterojunction by stacking n-type β-Ga_2O_3 nanobelts over p-type Si because it is challenging to obtain p-type β-Ga_2O_3 due to the intrinsic oxygen vacancies. The optical and electrical properties of the fabricated p-n heterojunction diodes were systematically investigated, illustrating the high potential of β-Ga_2O_3-based (opto)electronic devices.

EXPERIMENTAL DETAILS

A schematic of the device fabrication process is shown in Fig. 1. SiO_2/p^{++}Si (300 nm/500 μm) was partially covered with photoresist (PR) and immersed in a buffered oxide etchant (6 : 1 diluted HF, BOE, J.T. Baker) for 10 min at room temperature (Fig. 1(a)). The exposed SiO_2 was wet-etched to reveal the underlying p^{++}Si, which

†To whom correspondence should be addressed.
E-mail: hyunhyun7@korea.ac.kr

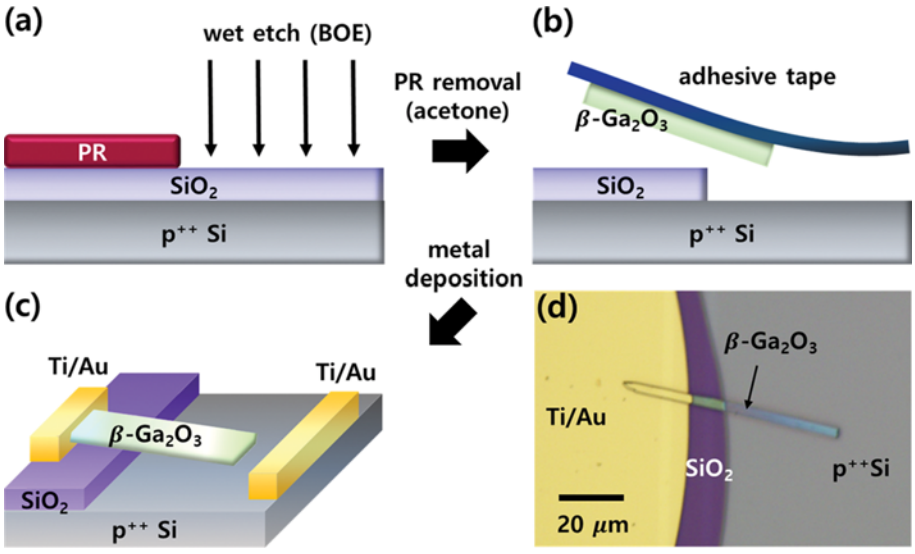

Fig. 1. (a)-(c) Schematic of device fabrication process, (d) optical microscope image of the fabricated p-n heterojunction diode.

was verified through sheet resistance measurements using a four-point probe (Desk 205, MS Tech) linked to a source meter (Keithley 2400). The microscale β-Ga_2O_3 nanobelts were mechanically exfoliated by using a commercial adhesive tape from the unintentionally n-doped bulk β-Ga_2O_3 single crystals (Tamura Corporation) grown by EFG. The mechanically exfoliated nanobelts were transferred onto the pre-patterned $SiO_2/p^{++}Si$ (Fig. 1(b)). As shown in Fig. 1(c), one end of the deposited β-Ga_2O_3 flake forms a p-n junction with the $p^{++}Si$ through van der Waals interactions, and the other end is isolated from the Si by the SiO_2 (300 nm thick). A conventional photolithography process and an electron beam evaporation technique were used to define Ti/Au contacts (100 nm/200 nm).

Fabrication of the β-Ga_2O_3/Si p-n heterojunction was confirmed using a combination of optical microscopy (Olympus, BX51M), field emission scanning electron microscopy (FE-SEM, Hitachi, S-4700), and electrical characterizations. Micro-Raman spectroscopy was conducted at room temperature in a back-scattering geometry with a 532 nm wavelength diode-pumped solid-state laser (Omicron) for analyzing the crystalline structure of the exfoliated β-Ga_2O_3 flake. Transmission electron microscopy (TEM, JEOL, JEM-2100F) and selected area electron diffraction (SAED) were also used to investigate the crystal structure and quality of the exfoliated nanobelts, where the specimen was prepared by focused ion beam milling (FIB, Quanta2003D, FEI). An additional carbon layer was deposited above the specimen to protect the surface of the sample from Ga-ion bombardments during FIB milling. The current-voltage (I-V) characteristics and time-dependent photoresponses were measured using a semiconductor parameter analyzer (Agilent 4155C) connected to the probe station. The UV lamp (15 W, UV Itec LTD) used as the light source had emission wavelengths of 254 and 365 nm. The light intensity was measured by using a power meter (FieldMax II-TO, Coherent). A Hall effect measurement system (Ecopia, HMS-3000) was used to determine the carrier concentration of the $p^{++}Si$ substrate.

RESULTS AND DISCUSSION

The optical microscope image in Fig. 1(d) shows that one end of the β-Ga_2O_3 flake lying on the SiO_2 is covered with Ti/Au and the opposite end contacts the $p^{++}Si$ substrate. The heterojunction structure was observed from several different viewpoints using FE-SEM. (Fig. 2(a)). The space between the transferred β-Ga_2O_3 flake and Si becomes smaller and eventually they form a heterojunction at the end. The three phonon peaks below 200 cm^{-1} are correlated to the low-frequency vibration and translation of tetrahedron-octahedron chains within the β-Ga_2O_3 structure (Fig. 2(b)). The

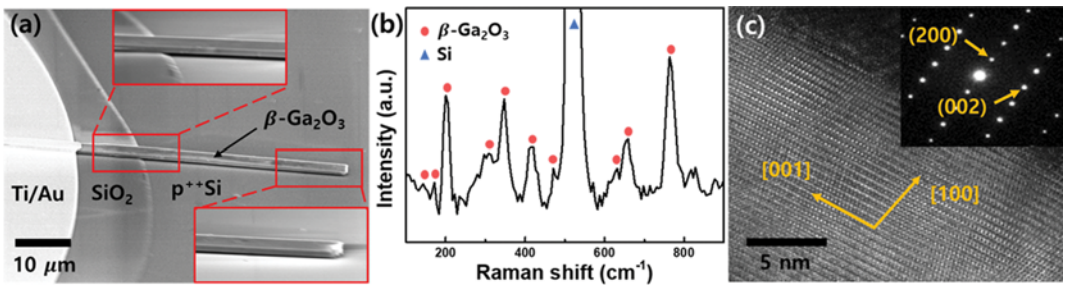

Fig. 2. (a) SEM images of the fabricated p-n β-Ga_2O_3/Si heterojunction diode, (b) micro-Raman spectrum of the exfoliated β-Ga_2O_3 flake, (c) TEM image and SAED pattern (inset) of the exfoliated β-Ga_2O_3 flake.

phonon peaks between 300 and 500 cm^{-1} are related to the mid-frequency deformation of Ga_2O_6 octahedra, and the peaks between 600 and 800 cm^{-1} are attributed to the high-frequency stretching and bending of GaO_4 tetrahedra (Fig. 2(b)) [21,22]. The peak positions in Fig. 2(b) are consistent with those reported in previous studies [21-23], which indicates that the quality of the β-Ga_2O_3 flakes was maintained during mechanical exfoliation, transfer, and device fabrication. A high-resolution cross-sectional TEM image and SAED pattern of the transferred β-Ga_2O_3 nanobelts was obtained. The surface of the exfoliated flakes had a crystallographic orientation of (100). It has already been shown that the atomic arrangement of monoclinic β-Ga_2O_3 permits facile cleavage into thin flakes along the [100] direction, which has a larger lattice constant than the other primary directions (a[100]=12.225 Å and b[010]=3.039 Å, c[001]=5.801 Å) [23,24]. Distances of 0.57 nm and 0.28 nm were calculated (inset of Fig. 2(c)) from the SAED pattern, corresponding to the distances between the (200) planes and (002) planes, respectively.

To investigate the electrical and optical properties of the β-Ga_2O_3/Si heterojunction p-n diodes, I-V measurements were conducted in both dark and light conditions (Fig. 3(a)). The diodes showed typical rectifying behavior. The asymmetric ratio (I_F/I_R) under dark conditions was as high as 1.56×10^4, with the current (I_R) at a reverse bias of −20 V and the current (I_F) at a forward bias of +20 V. The ideality factor was estimated to be approximately eight, which is attributed to the large series resistance, non-optimized contacts, and residues at the interface. The currents under 365 nm wavelength were the same as those under dark conditions, suggesting that the β-Ga_2O_3/Si heterojunction does not respond to the 365 nm wavelength (UV-A) (inset of Fig. 3(a)). However, it responded to the 254 nm wavelength (UV-C), indicating solar blindness of the fabricated p-n heterojunction.

The time-dependent photoresponses under 254 nm and 365 nm illuminations were also obtained at a forward bias of 30 V. The currents increased instantaneously from ~23 nA to ~55 nA during the exposure to 254 nm and decayed promptly to ~30 nA when the light source was off (Fig. 3(b)). However, no changes in the photocurrent were observed under illumination at 365 nm, which is different from other reported β-Ga_2O_3 photodetectors [7,8,25,26] that respond to the 365 nm wavelength to some extent. When deep-level defects are present, the wavelengths longer than the bandgap energy can be absorbed. The absence of photoresponse at the wavelength of 365 nm indicates high quality materials and a good junction between the n-type β-Ga_2O_3 and p-type Si.

For the time-dependent photoresponses, the fast-response (rise and decay) component is generally attributed to a rapid change in the photo-generated carrier concentrations when the light is turned on and off. Whereas, the slow-response component is related to the carrier trapping/de-trapping mechanism resulting from deep-level defects [26,27]. For a more detailed study of response time, a quantitative analysis of the current rise and decay process was conducted. The photoresponse curve was fitted with a bi-exponential relaxation function

$$I = I_0 + Ae^{-t/\tau_1} + Be^{-t/\tau_2}$$

where I_0 is the steady-state photocurrent, t is the time, A and B are constants, and τ_1 and τ_2 are two relaxation time constants. The photoresponse processes are well-fitted to the experimental data

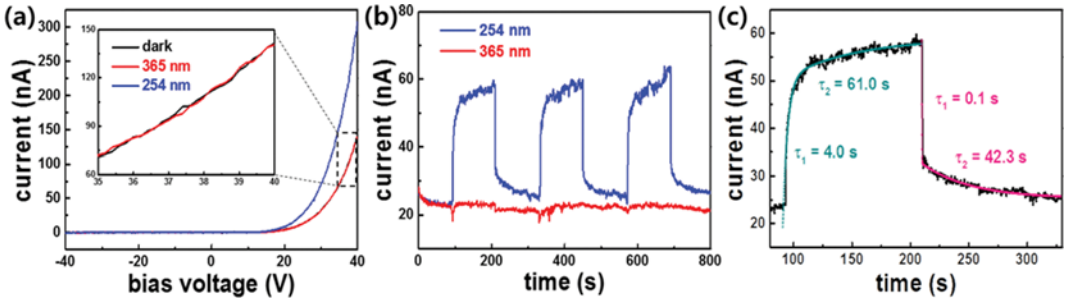

Fig. 3. Electrical and opto-optical properties of the fabricated p-n β-Ga_2O_3/Si heterojunction diode showing (a) I-V characteristics, (b) time-dependent photoresponse, and (c) experimental and fitted curve of photoresponse to 254 nm illumination.

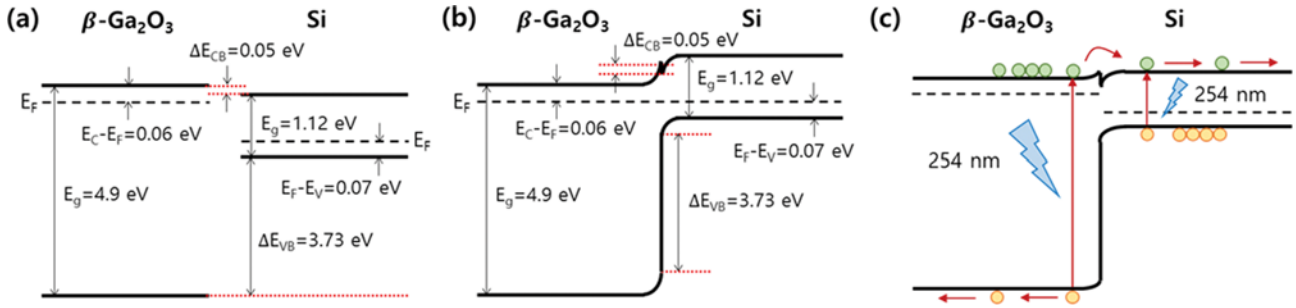

Fig. 4. Band diagrams of n-type β-Ga_2O_3 and p^{++} Si heterostructure showing (a) before junction formation, (b) after junction formation, and (c) under 254 nm illumination.

obtained under the illumination of 254 nm (Fig. 3(c)). Time relaxation constants under 254 nm exposure were 4.0 s (τ_1) and 61.0 s (τ_2), which are comparable to previous reports. The time relaxation constants for decay were 0.1 s (τ_1) and 42.3 s (τ_2), which can be attributed to the formation of the p-n heterojunction. The values of the conduction band offset (ΔE_{CB}) and valance band offset (ΔE_{VB}) were determined using Anderson's rule (Fig. 4) [29]. ΔE_{CB} was estimated to be 0.05 eV based on differences in electron affinities for β-Ga_2O_3 and Si, which were 4.0 eV and 4.05 eV, respectively. The ΔE_{VB} value was determined to be 3.73 eV based on the bandgap values of β-Ga_2O_3 and Si, which were 4.9 eV and 1.12 eV, respectively. Chen et al. used X-ray photoelectron spectroscopy to measure the valance and conduction band offsets for β-Ga_2O_3 and Si [30], and the values were similar to those reported here. The E_F-E_C value of β-Ga_2O_3 was estimated to be 0.06 eV, which is consistent with literature [31,32]. In the same way, the E_F-E_V value of Si is calculated to be 0.07 eV with a hole carrier concentration of 7.59×10^{17} cm^{-3}, measured by the Hall effect method. Considering all the values, the band diagrams of β-Ga_2O_3 and Si before and after junction formation are shown in Fig. 4(a) and (b), respectively. Type-II band alignment is assumed at the interface of the β-Ga_2O_3/Si heterojunction (Fig. 4(b)). The electron-hole pairs excited by 254 nm wavelength contributed to the photocurrent (Fig. 4(c)), demonstrating the p-n heterojunction solar-blind photodetectors.

CONCLUSION

Heterojunction p-n diodes with high rectification ratio, high spectral selectivity, and fast photoresponse were fabricated using n-type β-Ga_2O_3 micro-flake and p-type Si substrate. The micro-flakes mechanically exfoliated from single crystal β-Ga_2O_3 were transferred onto the p-Si substrate, forming a p-n junction by van der Waals interactions. The p-n heterojunction exhibited typical rectifying characteristics with a high rectification ratio of 1.56×10^4. A fast photo response to a wavelength of 254 nm (UV-C) was observed with no persistent photo conductance. Ga_2O_3-based optoelectronic devices can open up the possibility for next-generation solar-blind photodetectors.

ACKNOWLEDGEMENTS

The research was supported by the LG Innotek-Korea University Nano-Photonics Program, the Korea Institute of Energy Technology Evaluation and Planning (KETEP) and the Ministry of Trade, Industry & Energy (MOTIE) of Korea (No. 20153030012110) and Space Core Technology Development Program (2017M1A3A3A02015033) through the National Research Foundation of Korea funded by the Ministry of Science, ICT and Future Planning of Korea.

REFERENCES

1. T. Onuma, S. Saito, K. Sasaki, T. Masui, T. Yamaguchi, T. Honda and M. Higashiwaki, *Japan J. Appl. Phys.*, **54**, 112601 (2015).
2. H. He, R. Orlando, M. Blanco, R. Pandey, E. Amzallag, I. Baraille and M. Rerat, *Phys. Rev. B*, **74**, 195123 (2006).
3. M. Higashiwaki, K. Sasaki, A. Kuramata, T. Masui and S. Yamakoshi, *Appl. Phys. Lett.*, **100**, 013504 (2012).
4. M. A. Mastro, A. Kuramata, J. Calkins, J. Kim, F. Ren and S. J. Pearton, *ESC J. Solid State Sci. Technol.*, **6**(5), 356 (2017).
5. K. Sasaki, M. Higashiwaki, A. Kuramat, T. Masui and S. Yamakoshi, *J. Cryst. Growth*, **378**, 591 (2013).
6. M. Higashiwaki, K. Sasaki, T. Kamimura, M. H. Wong, D. Krishnamurthy, A. Kuramata, T. Masui and S. Yamakoshi, *Appl. Phys. Lett.*, **103**, 123511 (2013).
7. Y. H. An, D. Y. Guo, S. Y. Li, Z. P. Wu, Y. Q. Huang, P. G. Li, L. H. Li and W. H. Tang, *J. Phys. D: Appl. Phys.*, **49**, 285111 (2016).
8. D. Y. Guo, H. Z. Shi, Y. P. Qian, M. Lv, P. G. Li, Y. L. Su, Q. Liu, K. Chen, S. L. Wang, C. Cui, C. R. Li and W. H. Tang, *Semicond. Sci. Technol.*, **32**, 03LT01 (2017).
9. W.-Y. Kong, G.-A. Wu, K.-Y. Wang, T.-F. Zhang, Y.-F. Zou, D.-D. Wang and L.-B. Luo, *Adv. Mater.*, **28**, 10725 (2016).
10. Z. Chen, X. Wang, F. Zhang, S. Noda, K. Saito, T. Tanaka, M. Nishio, M. Arita and Q. Guo, *Appl. Phys. Lett.*, **109**, 022107 (2016).
11. F. Qian, S. Gradecak, Y. Li, C.-Y. Wen and C. M. Lieber, *Nano Lett.*, **5**, 2287 (2005).
12. Y. Hou, J.-S. Kim, S. Ashkenazi, M. O'Donnell and L. Guo, *Appl. Phys. Lett.*, **89**, 093901 (2006).
13. W. Lupan, V. V. Ursaki, G. Chai, L. Chow, G. A. Emelchenko, I. M. Tiginyanu, A. N. Gruzintsev and A. N. Redkin, *Sens. Actuators B: Chem.*, **144**, 56 (2010).
14. Y. B. Li, T. Tokizona, M. Y. Liao, M. Zhong, Y. Koide, I. Yamada and J. J. Delaunay, *Adv. Funct. Mater.*, **20**, 3972 (2010).
15. R. J. Zou, Z. Y. Zhang, Q. Liu, J. Q. Hu, L. W. Sang, M. Y. Liao and W. J. Zhang, *Small*, **10**, 1848 (2014).
16. L. Li, E. Auer, M. Y. Liao, X. S. Fang, T. Y Zhai, U. K. Gautam, A. Lugstein, Y. Koide, Y. Bando and D. Golberg, *Nanoscale*, **3**, 1120 (2011).
17. W. Tian, C. Y. Zhi, T. Y. Zhai, S. M. Chen, X. Wang, M. Y. Liao, D. Golberg and Y. Bando, *J. Mater. Chem.*, **22**, 17984 (2012).
18. W. Feng, X. N. Wang, J. Zhang, L. F. Wang and B. Yang, *J. Mater. Chem.*, **2**, 3254 (2014).
19. G.-H. Lee, Y.-J. Yu, X. Cui, N. Petrone, C.-H. Lee, M. S. Choi, D.-Y. Lee, C. Lee, W. J. Yoo, K. Watanabe, T. Taniguchi, C. Nuckolls, P. Kim and J. Hone, *ACS Nano*, **7**(9), 7931 (2013).
20. Z. Feng, B. Chen, S. Qian, L. Xu, L. Feng, Y. Yu, R. Zhang, J. Chen, Q. Li, Q. Li, C. Sun, H. Zhang, J. Liu, W. Pang and D. Zhang, *2D Mater.*, **3**, 035021 (2016).
21. S. Kumar, G. Sarau, C. Tessarek, M. Y. Bashouti, A. Hähnel, S. Christiansen and R. Singh, *J. Phys. D: Appl. Phys.*, **47**, 435101 (2014).
22. S. Oh, J. Kim, F. Ren, S. J. Pearton and J. Kim, *J. Mater. Chem. C*, **4**, 9245 (2016).
23. J. Kim, S. Oh, M. A. Mastro and J. Kim, *Phys. Chem. Chem. Phys.*, **18**, 15760 (2016).
24. J. Ahman, G. Svensson and J. Albertsson, *Acta Crystallogr., Sect. A: Cryst. Phys. Diffr. Theor. Gen. Crystallogr.*, **52**, 1336 (1996).
25. X. C. Guo, N. H. Hao, D. Y. Guo, Z. P. Wu, Y. H. An, X. L. Chu, L. H. Li, P. G. Li, M. Lei and W. H. Tang, *J. Alloys and Compounds*, **660**, 136 (2016).
26. D. Guo, Z. Wu, P. Li, Y. An, H. Liu, X. Guo, H. Yan, G. Wang, C. Sun, L. Li and W. Tang, *Opt. Mater. Express.*, **4**, 1067 (2014).
27. D. Y. Guo, Z. P. Wu, Y. H. An, X. C. Guo, X. L. Chu, C. L. Sun, L. H.

Li, P. G. Li and W. H. Tang, *Appl. Phys. Lett.*, **105**, 023507 (2014).
28. Y. Kwon, G. Lee, S. Oh, J. Kim, S. J. Pearton and F. Ren, *Appl. Phys. Lett.*, **110**, 131901 (2017).
29. S. M. Sze and K. K. Ng, *Physics of Semiconductor Devices*, 3rd Ed., Wiley-Interscience (2007).
30. Z. Chen, K. Nishihagi, X. Wang, K. Saito, T. Tanaka, M. Nishio, M. Arita and Q. Guo, *Appl. Phys. Lett.*, **109**, 102106 (2016).
31. T. C. Lovejoy, R. Chen, X. Zheng, E. G. Villora, K. Shimamura, H. Yoshikawa, Y. Yamashita, S. Ueda, K. Kobayashi, S. T. Dunham, F. S. Ohuchi and M. A. Olmstead, *Appl. Phys. Lett.*, **100**, 181602 (2012).
32. Y. Kokubun, S. Kubo and S. Nakagomi, *Appl. Phys. Express.*, **9**, 091101 (2016).